

Research papers

Estimating uncertainty and its temporal variation related to global climate models in quantifying climate change impacts on hydrology



Mingxi Shen^a, Jie Chen^{a,*}, Meijia Zhuan^a, Hua Chen^a, Chong-Yu Xu^{a,b}, Lihua Xiong^a

^a State Key Laboratory of Water Resources and Hydropower Engineering Science, Wuhan University, Wuhan 430072, China

^b Department of Geosciences, University of Oslo, P.O. Box 1047 Blindern, N-0316 Oslo, Norway

ARTICLE INFO

Article history:

Received 25 April 2017

Received in revised form 1 November 2017

Accepted 3 November 2017

Available online 6 November 2017

This manuscript was handled by Marco Borga, Editor-in-Chief, with the assistance of Hamid Moradkhani, Associate Editor

Keywords:

Climate change

Hydrology

Uncertainty

Global climate model

Temporal variation

ABSTRACT

Uncertainty estimation of climate change impacts on hydrology has received much attention in the research community. The choice of a global climate model (GCM) is usually considered as the largest contributor to the uncertainty of climate change impacts. The temporal variation of GCM uncertainty needs to be investigated for making long-term decisions to deal with climate change. Accordingly, this study investigated the temporal variation (mainly long-term) of uncertainty related to the choice of a GCM in predicting climate change impacts on hydrology by using multi-GCMs over multiple continuous future periods. Specifically, twenty CMIP5 GCMs under RCP4.5 and RCP8.5 emission scenarios were adapted to adequately represent this uncertainty envelope, fifty-one 30-year future periods moving from 2021 to 2100 with 1-year interval were produced to express the temporal variation. Future climatic and hydrological regimes over all future periods were compared to those in the reference period (1971–2000) using a set of metrics, including mean and extremes. The periodicity of climatic and hydrological changes and their uncertainty were analyzed using wavelet analysis, while the trend was analyzed using Mann-Kendall trend test and regression analysis. The results showed that both future climate change (precipitation and temperature) and hydrological response predicted by the twenty GCMs were highly uncertain, and the uncertainty increased significantly over time. For example, the change of mean annual precipitation increased from 1.4% in 2021–2050 to 6.5% in 2071–2100 for RCP4.5 in terms of the median value of multi-models, but the projected uncertainty reached 21.7% in 2021–2050 and 25.1% in 2071–2100 for RCP4.5. The uncertainty under a high emission scenario (RCP8.5) was much larger than that under a relatively low emission scenario (RCP4.5). Almost all climatic and hydrological regimes and their uncertainty did not show significant periodicity at the $P = .05$ significance level, but their temporal variation could be well modeled by using the fourth-order polynomial. Overall, this study further emphasized the importance of using multiple GCMs for studying climate change impacts on hydrology. Furthermore, the temporal variation of uncertainty sourced from GCMs should be given more attention.

© 2017 Elsevier B.V. All rights reserved.

1. Introduction

Various sources of uncertainty have been identified in the process of assessing climate change impacts on hydrology (Wilby and Harris, 2006; Chen et al., 2011b). Understanding, quantifying and reducing the uncertainty become crucial to water resource management. Generally, the uncertainty mainly comes from: (1) greenhouse gas emission scenario (GHGES) (e.g. Maurer, 2007; Nobrega et al., 2011; Fang et al., 2015; Ficklin et al., 2016); (2) global climate model (GCM) (e.g. Jenkins and Lowe, 2003; Rowell, 2006; Teng et al., 2012; Chen et al., 2012); (3) natural climate variability (e.g.

Hawkins and Sutton, 2009; Brisson et al., 2015; Chen et al., 2016); (4) downscaling method (e.g. Wilby et al., 1998; Fowler et al., 2007; Samadi et al., 2013; Etemadi et al., 2014; Li et al., 2015); and (5) hydrological model structure and parameter (e.g. Poulin et al., 2011; Bae et al., 2011; Brigode et al., 2013; Eregno et al., 2013; Jiang et al., 2007).

Many studies have involved in quantifying the uncertainty of climate change impacts on hydrology arising from above sources. Especially, the uncertainty related to GCM and GHGES has been extensively studied during the last decade. For example, Maurer (2007) investigated the uncertainty related to the choice of a GCM and GHGES in assessing the hydrological impacts of climate change in the Sierra Nevada (California) by using eleven GCMs under two emission scenarios. Nobrega et al. (2011) quantified

* Corresponding author.

E-mail address: jiechen@whu.edu.cn (J. Chen).

the uncertainty of climate change impacts on the discharge of Rio Grande in South America by using six GCMs and four emission scenarios. Minville et al. (2008) employed five GCMs and two GHGESs to implement the same investigation over a Nordic watershed. These studies found that both GCM and GHGES contribute great uncertainty to the hydrological impacts of climate change. The uncertainty of downscaling has also been investigated in several studies. For example, Mpelasoka and Chiew (2009) compared three downscaling methods in constructing future runoff across Australia; Chen et al. (2011a) compared six downscaling methods in simulating the future streamflow of a Canadian watershed. They found that the uncertainty related to the downscaling method could be significant when quantifying climate change impacts on hydrology, especially for extremes. Studies have also investigated the uncertainty of hydrological modeling when assessing climate change impacts on hydrology. For example, Jiang et al. (2007) compared six monthly water balance models in investigating the potential impacts of climate change on the water availability of a Chinese basin; Teng et al. (2012) used five lumped conceptual daily rainfall-runoff models to simulate climate change impacts on the runoff across southeast Australia. Their results indicated that hydrological model could lead to significant uncertainty in the prediction of future runoff.

In addition to the investigation of each individual uncertainty source, several studies also compared the uncertainty from different sources in the assessment of hydrological climate change impacts. For example, Wilby and Harris (2006) compared five uncertainty sources in the prediction of low-flows for the River Thames (UK) by using four GCMs, two GHGESs, two statistical downscaling techniques, two hydrological model structures and two sets of hydrological model parameters. Their results indicated that the choice of a GCM is the largest contributor to uncertainty, followed by the downscaling method, and uncertainty related to hydrological modeling and emission scenario is relatively less important. Prudhomme and Davies (2009) employed three GCMs, two GHGESs and two downscaling techniques (statistical downscaling model (SDSM) and dynamical downscaling model (RCM HadRM3)) to investigate the uncertainty of climate change impacts on the river flow of four British catchments. They also found that GCM is the largest source of uncertainty, while uncertainty related to downscaling technique and emission scenario is of similar magnitude, but generally smaller than that related to GCM. Similarly, Chen et al. (2011b) conducted a comprehensive study of uncertainty using two GHGESs, six GCMs, a five-member ensemble of a GCM, four downscaling techniques, three hydrological model structures and ten sets of hydrological model parameters. The results showed that the choice of a GCM is a major contributor to uncertainty, followed by downscaling method, GHGES and hydrological model structure. The contribution of hydrological model parameters is less important. All above studies consistently show that the choice of a GCM is the largest contributor to overall uncertainty of hydrological climate change impact studies. Thus, the use of a multi-model ensemble is recommended when implementing climate change studies (Minville et al., 2008; Zhang et al., 2011; Teng et al., 2012).

Although lots of studies have explored the uncertainty of climate change as well as its impacts, studies focusing on the temporal variation of uncertainty are relatively fewer, and most are qualitative studies. For example, Hawkins and Sutton (2009, 2011) investigated the temporal variation of uncertainty sourced from internal variability, climate model, emission scenarios for the 21st century. Jung et al. (2012) compared the uncertainty of climate model, hydrological model parameter and emission scenario from ten 20-year time-slice periods in 2000–2099 for two river basins in the Pacific Northwest of US. Ahmadalipour et al. (2017) characterized the uncertainty from climate model, downscaling and emis-

sion scenarios for period 2010–2099 when assessing the climate changes over Columbia River basin. The results of above studies showed that the uncertainty from various sources would vary over time, and the uncertainty derived from one source might dominate in one period, while that derived from the other source might prevail in the other period.

But beyond that, some important questions or puzzles still need to be solved when assessing the hydrological impacts of climate change, such as, how does the uncertainty caused by single source propagate over time? How to quantify the temporal variation of uncertainty? Answers to such questions would contribute to a more reliable climate change projection, as well as better strategies dealing with climate change.

Therefore, this study investigated and estimated the temporal variation (mainly long-term) of uncertainty stemming from the major contributor – the choice of a GCM – in assessing the hydrological impacts of climate change. To achieve this, twenty CMIP5 GCMs under two emission scenarios (RCP4.5 and RCP8.5) were adopted to adequately represent this uncertainty envelope, fifty-one 30-year continuous future horizons obtained by moving a 30-year window from 2021 to 2100 with 1-year interval were used to express the temporal variation of uncertainty. The temporal variation was analyzed by a set of statistical approaches, such as wavelet analysis, Mann-Kendall trend test and polynomial regression analysis.

The paper is structured as follows: a brief description of the studied area and data is presented in Section 2, followed by a detailed description of the bias correction method, hydrological model and data analysis approach in Section 3. Section 4 elaborates on the results by analyzing the climatic and hydrologic changes and their uncertainty over 51 future periods. Finally, the discussion and conclusion are provided in Section 5.

2. Study area and data

2.1. Study area

The proposed approach (described in Section 3) is conducted on the Hanjiang River watershed (Fig. 1), which is located in the south-central China. The river originates from the southern Qinling Mountain, flows through Shanxi and Hubei Provinces, and finally merges into the Yangtze River (the longest river in Asia) in Wuhan city, with a main stream length of 1577 km and a drainage area of 159,000 km². In the Hanjiang River watershed, the annual mean temperature is about 15.5 °C and the annual average rainfall is 873 mm (Chen et al., 2012). The watershed has a subtropical mon-

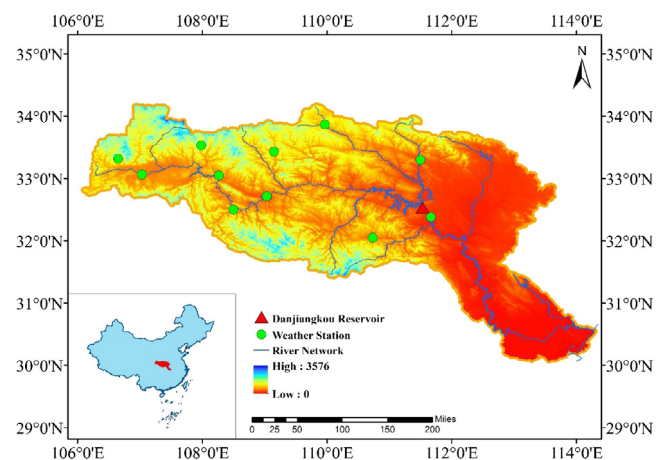


Fig. 1. Location map of the Hanjiang River watershed.

soon climate, in which the precipitation is mainly caused by the southeastern and southwestern maritime monsoons. Seventy-five percent of its total precipitation occurs between June and October, during this time the prolonged rainfalls in autumn and rainstorms in early summer often cause major floods (Xu et al., 2012). The annual mean discharge of the Hanjiang River is about 1150 m³/s (Wang et al., 2015). In the middle of the Hanjiang River watershed, there locates the Danjiangkou Reservoir, which serves as a water source for the Middle Route of the South-to-North Water Transfer Project (MSWTP). The sub-basin above the Danjiangkou Reservoir with a drainage area of 89,540 km² is used in this study. The MSWTP has relieved chronic water shortage problems in several provinces and cities of China including the capital Beijing. This is a crucial motivating factor for understanding the uncertainty and its temporal variation of climate change impacts on the hydrology over this watershed, as it will be vital for making water diversion decisions for this watershed in the future.

2.2. Data

This study used both observed and GCM-simulated daily precipitation (prcp), minimum and maximum temperature (Tmin, Tmax) data in the Hanjiang River watershed. The observed data covered 1971–2000 for the historical period, the GCMs covered 1971–2000 for the history and 2021–2100 for the future. Observed meteorological data from eleven weather stations were obtained from the China Meteorological Data Sharing Service System. The streamflow at the sub-basin outlet is the inflow of the Danjiangkou Reservoir, which was provided by the Bureau of Hydrology of the Changjiang Water Resources Commission. The climate model simulations were taken from the Coupled Model Intercomparison Project Phase 5 (CMIP5) database. Twenty GCMs under two GHGSS (RCP4.5 and RCP8.5) from fourteen modeling centres were selected to adequately represent the uncertainty of climate models. Table 1 presents the general information of these twenty GCMs. In order to run a lumped hydrological model, the precipitation and temperature data from both observations and GCM simulations were averaged over several grid boxes within and surrounding the

watershed to a single time series using the Thiessen polygon method.

3. Methodology

3.1. Bias correction method

GCM outputs are usually too coarse to directly drive a hydrological model for hydrological climate change impact studies, in this case, a downscaling or bias correction technique must be utilized (Xu, 1999; Chen et al., 2011a; Jung et al., 2012). This study used a bias correction method for its simplicity and good performance (Teng et al., 2012; Jung et al., 2012; Ahmadalipour et al., 2017).

The used bias correction method is the Daily Bias Correction method (DBC, Chen et al., 2013), which is a hybrid, advanced bias correction method combining the Local intensity scaling method (LOCI, Schmidli et al., 2006) and the Daily translation method (DT, Mpelasoka and Chiew, 2009) to correct both the wet day frequency and the distribution of wet day precipitation. The DBC method first takes advantage of the LOCI method to correct the precipitation occurrence, and then, instead of applying the same factor (LOCI) to scale daily precipitation for a particular month, it adopts the DT method to modulate the changes as a function of the percentile differences in the frequency distribution of precipitation (or temperature) between observation and climate model. More details are as follows:

(1) For a particular month (e.g. January) in the reference period, a wet-day threshold is determined from the GCM to ensure that the threshold exceedance equals the observed wet-day frequency for that month; (2) the threshold is then applied to the future period to correct the GCM's precipitation in corresponding month; (3) a relationship between observation and GCM is established using the distribution mapping technique by calculating the percentiles (100 percentile values from the 1st to the 100th percentile in this study) of daily precipitation (temperature) in the reference period. In other words, the distributions of observation and GCM are represented by 100 percentile values; and (4) the percentile ratios of precipitation are multiplied by the GCM precipitation series in

Table 1
General information of the chosen GCMs.

ID	Model name	Modeling centre	Institution	Horizontal resolution (lon. × lat.)
1	ACCESS1.0	CSIRO-BOM	CSIRO (Commonwealth Scientific and Industrial Research Organisation, Australia), and BOM (Bureau of Meteorology, Australia)	1.875 × 1.25
2	ACCESS1.3			1.875 × 1.25
3	BCC-CSM1.1 (m)	BCC	Beijing Climate Center, China Meteorological Administration	1.125 × 1.125
4	BCC-CSM1.1			2.8 × 2.8
5	BNU-ESM	GCESS	College of Global Change and Earth System Science, Beijing Normal University	2.8 × 2.8
6	CanESM2	CCCma	Canadian Centre for Climate Modelling and Analysis	2.8 × 2.8
7	CMCC-CMS	CMCC	Centro Euro-Mediterraneo per I Cambiamenti Climatici	1.875 × 1.875
8	CNRM-CM5	CNRM-CERFACS	Centre National de Recherches Meteorologiques/Centre Europeen de Recherche et Formation Avancees en Calcul Scientifique	1.4 × 1.4
9	CSIRO-Mk3.6.0	CSIRO-QCCCE	Commonwealth Scientific and Industrial Research Organisation in collaboration with the Queensland Climate Change Centre of Excellence	1.8 × 1.8
10	FGOALS-g2	LASG-CESS	LASG, Institute of Atmospheric Physics, Chinese Academy of Sciences; and CESS, Tsinghua University	1.875 × 1.25
11	GFDL-ESM2G	NOAA-GFDL	Geophysical Fluid Dynamics Laboratory	2.5 × 2.0
12	GFDL-ESM2M			2.5 × 2.0
13	INMCM4	INM	Institute for Numerical Mathematics	2.0 × 1.5
14	IPSL-CM5A-LR	IPSL	Institut Pierre-Simon Laplace	3.75 × 1.8
15	IPSL-CM5A-MR			2.5 × 1.25
16	IPSL-CM5B-LR			3.75 × 1.8
17	MIROC5	MIROC	Atmosphere and Ocean Research Institute (The University of Tokyo), National Institute for Environmental Studies, and Japan Agency for Marine-Earth Science and Technology	1.4 × 1.4
18	MIROC-ESM-CHEM	MIROC	Japan Agency for Marine-Earth Science and Technology, Atmosphere and Ocean Research Institute (The University of Tokyo), and National Institute for Environmental Studies	2.8 × 2.8
19	MIROC-ESM			2.8 × 2.8
20	MRI-CGCM3	MRI	Meteorological Research Institute	1.1 × 1.1

the future period (or the percentile differences are added to the GCM temperature series in the future period) (Eq. (1))

$$X_{\text{cor},j} = F_o^{-1}(F_m(X_{\text{fut},j})) \quad (1)$$

where X refers to precipitation or temperature, *fut* means variable in the future period, *cor* means corrected variable, the subscript j refers to a specific day in the future period, F_m is the Cumulative Distribution Function (CDF, represented by 100 percentile values from the 1st to the 100th) of simulated precipitation (or temperature) in the reference period, and F_o^{-1} is the inverse CDF of the observed precipitation (or temperature) in the reference period.

For every GCM, the DBC method was first calibrated in the reference period (i.e. find the GCM wet-day threshold for every month and construct the distribution relationships between observation and GCM), and then the calibrated DBC was applied to correct GCM's precipitation and temperature for all fifty-one future periods, which are 2021–2050 (2035s), 2022–2051 (2036s), 2023–2052 (2037s), ..., 2070–2099 (2084s) and 2071–2100 (2085s). Note that these future periods were corrected individually from each other. The fifty-one 30-year continuous future periods with 1-year interval filtered the short-term fluctuations and changes such as inter-annual variability, so they mainly reflected the long-term temporal variation of climatic and hydrological changes and their uncertainty. Additionally, when using a bias correction method, it is implicitly assumed that climate model's biases are stationary over time (Maraun, 2013; Chen et al., 2013).

3.2. Hydrological modeling

The hydrological model used in this study is the HMETs model (the Hydrological Model of École de technologie supérieure), which is a lumped conceptual rainfall-runoff model developed at the École de technologie supérieure, University of Quebec. It has been used in several flow forecasting and climate change impact studies (e.g. Chen et al., 2011b; Arsenault et al., 2014; Brigode et al., 2015).

HMETs uses two connected reservoirs representing unsaturated (i.e. vadose) and saturated (i.e. phreatic) zones, and simulates the basic hydrological processes of snow accumulation, melting and refreezing, evapotranspiration, infiltration as well as flow routing to the watershed outlet (Martel et al., 2017; Troin et al., 2015). The model begins with a snowmelt module which works in three steps: overnight refreezing, snowmelt and snowpack water retention capacity. The water in the snowpack is from snowmelt and liquid precipitation. If the amount of water in the snowpack exceeds the water retention capacity, the remaining water is then added to the water available for runoff. A fraction of the water available for runoff will be directly taken as surface runoff. Once the surface runoff and real evapotranspiration are taken out, the remaining water for runoff will infiltrate to the vadose zone. In this process, a portion of the infiltrated water which depends on the water level of vadose zone is treated as delayed runoff component. The vadose zone offers water for the hypodermic flow component and the exchanges to the saturated zone. If the vadose zone fills up, the remaining water will be added to the delayed runoff component. The saturated zone is mainly used to release groundwater flow. If the saturated zone level exceeds the maximum, the exceeding water is also added to the delayed runoff component. Surface and delayed runoff are transferred to the outlet using two unit hydrographs, and are summarized to the hypodermic flow and the groundwater flow. Finally the total streamflow is used to represent the modeled streamflow.

HMETs has up to 21 parameters, which are shown in Table 2 (Martel et al., 2017). Model calibration is done automatically using the Covariance Matrix Adaptation Evolution Strategy (CMAES). This strategy is a continuous domain, non-convex, non-linear

problem optimization algorithm. It estimates the derivatives of the covariance matrix of the previously successful candidate solution distribution using the maximum-likelihood principle. In this way, it tends to maximize the likelihood of the distribution. More details of this optimization method can be found in Hansen and Ostermeier (2001) and Arsenault et al. (2014).

HMETs requires daily mean temperature and precipitation as inputs. If the maximum and minimum temperatures are input to the model, they are automatically averaged to mean temperature. A natural streamflow time series is also needed for model calibration. The optimal combination of parameters is chosen based on the Nash-Sutcliffe efficiency (NSE) criterion.

In this study, 20 years (1961–1980) of daily time series (precipitation, maximum and minimum temperature and flow) were used for model calibration and another 20 years (1981–2000) were used for model validation. The optimized parameters yielded Nash-Sutcliffe criterion values of 0.79 for calibration and 0.78 for validation, which shows that HMETs performs relatively well for this watershed at the daily time step. The observed and simulated mean hydrographs in Fig. 2 further demonstrate the reasonable performance of HMETs in this watershed.

3.3. Data analysis

The performance of the DBC method is first verified over the reference period (1971–2000) using nine climate statistics as criteria, which include the mean, standard deviation, 25th, 50th, 75th, 90th, 95th, and 99th percentiles and maximum of precipitation (or temperature) at different timescales (daily, monthly and annual). The relative differences between the corrected and observed precipitation series of these statistics were calculated (Eq. (2)), while the absolute differences were calculated for temperature (Eq. (3)):

Table 2

List of the HMETs model's parameters.

Parameter	Definition
<i>Snow model parameters (10 parameters)</i>	
ddf_{\min}	Minimum degree-day-factor in mm/°C/day
ddf_{plus}	Maximum degree-day-factor in mm/°C/day ($ddf_{\min} + ddf_{\text{plus}} = ddf_{\max}$)
T_{bm}	Base melting temperature in °C
K_{cum}	Empirical parameter for the calculation of the degree-day-factor in mm^{-1}
fc_{\min}	Minimum fraction for the snowpack water retention capacity
fc_{plus}	Maximum fraction of the snowpack water retention capacity ($fc_{\min} + fc_{\text{plus}} = fc_{\max}$)
C_{cum}	Parameter for the calculation of water retention capacity in mm^{-1}
T_{bf}	Base refreezing temperature in °C
K_f	Degree-day factor for refreezing in mm/°C/day
Fe	Empirical exponent for the freezing equation
<i>Real evapotranspiration (1 parameter)</i>	
ET_{eff}	Fraction of the potential evapotranspiration
<i>Subsurface (6 parameters)</i>	
C_r	Fraction of the water for surface and delayed runoff
C_{vp}	Fraction of the water for groundwater recharge
C_v	Fraction of the water for hypodermic flow
C_p	Fraction of the water for groundwater flow
LV_{\max}	Maximum level of the vadose zone in mm
LP_{\max}	Maximum level of the phreatic zone in mm
<i>Unit hydrograph parameters (4 parameters)</i>	
α_1	Shape parameter α for the gamma distribution used on the surface unit hydrograph
β_1	Rate parameter β for the gamma distribution used on the surface unit hydrograph
α_2	Shape parameter α for the gamma distribution used on the delayed unit hydrograph
β_2	Rate parameter β for the gamma distribution used on the delayed unit hydrograph

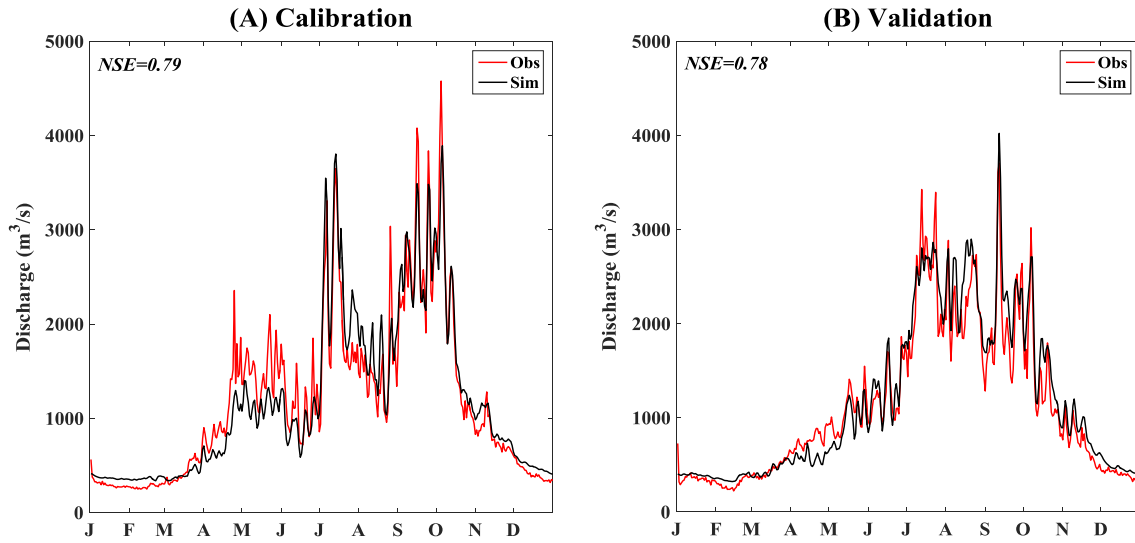


Fig. 2. Observed and modeled averaged hydrographs for (A) the calibration period (1961–1980) and (B) the validation period (1981–2000).

$$RD = (P_{cor} - P_{obs}) / P_{obs} \times 100\% \quad (2)$$

$$AD = T_{cor} - T_{obs} \quad (3)$$

where *RD* means relative difference, *AD* means absolute difference, P_{obs} , P_{cor} mean statistics of observed and corrected precipitation, respectively, T_{obs} , T_{cor} mean statistics of observed and corrected temperature, respectively.

For hydrological simulation, the corrected precipitation and temperature series in 51 future periods were used to drive the calibrated HMETS model. Fifty-one hydrological simulations were obtained by running the hydrological model 51 times using 51 future climate projections all based on the same calibrated parameters. The hydrological impacts of climate change were represented by three hydrological variables: mean flow, high flow (95th percentile of 30-year daily flow) and low flow (5th percentile of 30-year daily flow). The changes of these variables for future periods relative to the reference period were calculated. Since the hydrological model is not “perfect”, the simulated streamflow is slightly biased when comparing to observed counterpart. To get rid of the influence of the biases caused by the hydrological model, the model simulated future period streamflow was compared with the model simulated reference period streamflow rather than the gauged streamflow. This method has been widely used in previous studies (e.g. Minville et al., 2008; Chen et al., 2011a; Jung et al., 2012).

With the changes of future climate and hydrology (relative change for precipitation and discharge, and absolute change for temperature) from 20 GCMs and 51 future periods, the ensemble median (similar to ensemble mean) and its uncertainty for each period can be defined as illustrated in Fig. 3. The upper part of Fig. 3 presents the calculation of ensemble median and uncertainty for one future period: For example, in the future period 2021–2050, 20 GCMs could provide 20 different values in terms of the future change, the ensemble median is defined as the median value of the 20 predictions, and the uncertainty is defined as the range between the maximum and minimum predictions when excluding outliers. When illustrating with a boxplot (Fig. 3), the ensemble median in a future period is Q3 and the uncertainty is the range between the upper and lower boundaries (Q1–Q5). The ensemble median and uncertainty range have been widely used to represent the temporal variation of uncertainty in previous studies (e.g. Kharin et al., 2013; Sillmann et al., 2013; IPCC, 2013), even though resampling methods such as bootstrapping (Khan et al., 2006;

Samadi et al., 2013) can also be used to define uncertainty. Following this method, 51 ensemble medians and 51 uncertainty values were calculated for all 51 future periods to investigate the temporal variation of deterministic changes and their uncertainty (the lower part of Fig. 3).

Some data analysis techniques: wavelet analysis (Torrence and Compo, 1998; Xu et al., 2011), Mann-Kendall trend test (Mann, 1945; Kendall, 1975), and regression analysis (Bates and Watts, 1988) were used to analyze the temporal variation of deterministic changes and their uncertainty. Specifically, wavelet analysis was used to analyze the periodicity, and the Mann-Kendall trend test was applied to examine the trend. If the Mann-Kendall trend test revealed significant trend at the $P = .05$ significance level, then the regression analysis was applied to simulate the changing pattern of the time series. Besides, F-test was used to examine the significance of the regression model, and three indexes measured the performance of the regression model, including Willmott's refined index of agreement (d_r) (Willmott et al., 2012; Willmott et al., 2015), determination coefficient (R^2) (Ferraro et al., 2011), and mean absolute error (MAE) (Willmott and Matsuura, 2005). Eq. (4) gives the definition of d_r , which is at the range of -1.0 to 1.0 , a d_r value closer to 1 means better simulation.

$$d_r = \begin{cases} 1 - \frac{\sum_{i=1}^n |P_i - O_i|}{c \sum_{i=1}^n |O_i - \bar{O}|}, & \sum_{i=1}^n |P_i - O_i| \leq c \sum_{i=1}^n |O_i - \bar{O}| \\ \frac{c \sum_{i=1}^n |O_i - \bar{O}|}{\sum_{i=1}^n |P_i - O_i|} - 1, & \sum_{i=1}^n |P_i - O_i| > c \sum_{i=1}^n |O_i - \bar{O}| \end{cases} \quad (4)$$

where P_i is the model-derived prediction, O_i is the observation, n is the length of observations, and \bar{O} is the mean of the observations. Usually, c is equal to 2.0.

When applying wavelet analysis, choosing an appropriate wavelet is of great importance. The wavelet depends on the nature of the time series and on the type of information to be extracted (De Moortel et al., 2004). In this study, *morelet* was used based on its good localization in both time and frequency space (Torrence and Compo, 1998), and also based on the principles of self-similarity, compactness and smoothness (Ramsey, 1999). Since this study analyzes the periodicity of a time series, the Continuous Wavelet Transform (CWT) was applied. Statistical significance level of periodicity was estimated against a red noise model (Torrence and Compo, 1998; Grinsted et al., 2004). Free Matlab software package of wavelet analysis provided by Grinsted et al. (2004) was used to implement this analysis.

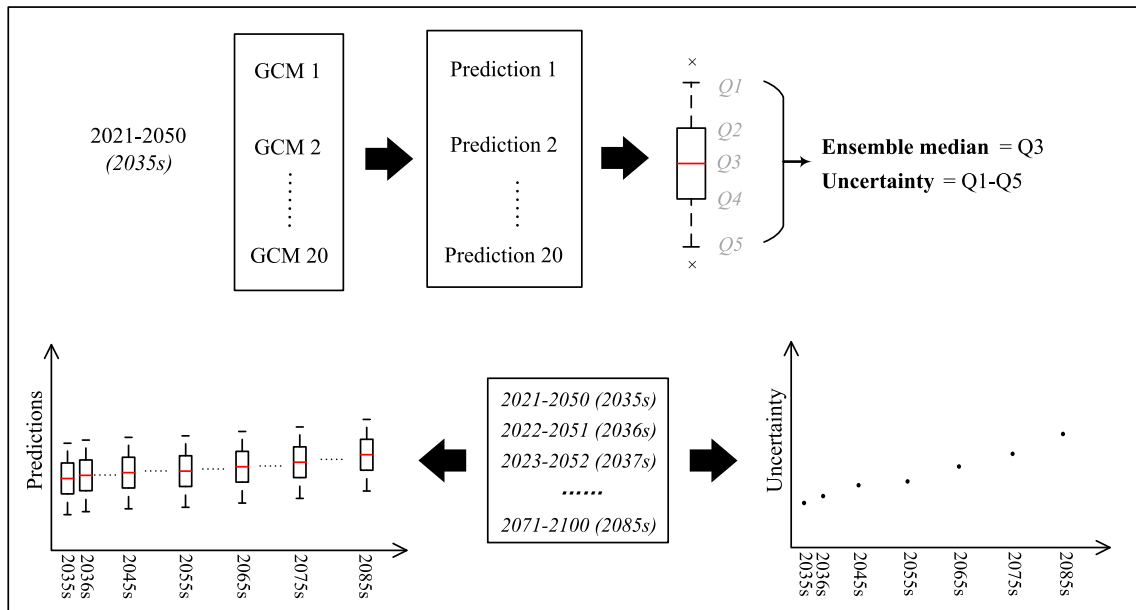


Fig. 3. Schematic illustrating of the general approach of defining ensemble median and uncertainty. In every boxplot, Q2 is the 75th percentile value of the twenty predictions, Q3 is the 50th percentile value (i.e. median), and Q4 is the 25th percentile value. Q2–Q4 is the interquartile range (IQR), Q1 is the upper boundary defined as $Q2 + 1.5 \times \text{IQR}$, Q5 is the lower boundary defined as $Q4 - 1.5 \times \text{IQR}$. Points are outliers if larger than Q1 or smaller than Q5. In this study, ensemble median is defined as the median value (Q3), and uncertainty is defined as the prediction range after excluding outliers (Q1–Q5).

When using regression analysis, considering the chaotic nature of climate system and nonstationarity of climate change, a linear model may not be a proper choice for modeling climatic and hydrologic changes and their uncertainty; referred to the studies of Hawkins and Sutton (Hawkins and Sutton, 2009; 2011), the fourth-order polynomial was used to fit the future climatic and hydrological changes and their uncertainty.

4. Results

4.1. Bias correction method verification

The performance of the DBC method was validated with respect to reproducing nine observed statistics. Fig. 4 presents the biases of raw and corrected GCMs' precipitation and temperature on the daily time scale in 1971–2000. In the figure, x-axis represents the 20 GCMs following the order in Table 1, y-axis represents the GCMs' biases in terms of reproducing nine statistics: mean, standard deviation, 25th, 50th, 75th, 90th, 95th, and 99th percentiles, and maximum value from number 1 to 9. Darker color means larger bias. From the figure, the raw GCMs were considerably biased in simulating precipitation and temperature. The biases in raw temperature series were above 2 °C (absolute value), and the biases in raw precipitation series were mostly above 15% (absolute value) in terms of the nine statistics. But after correction, the biases in precipitation considerably reduced to less than 5%. Particularly, the DBC method performed better for mean precipitation than for extremes. In addition, the DBC method considerably reduced the biases of GCM temperature for all statistics, especially for minimum temperature. All above results indicate the reasonable performance of the DBC method, justifying its use for generating future climate change scenarios for hydrological impact studies.

4.2. Climate change projection

4.2.1. Changes in annual precipitation and temperature

Fig. 5 shows the relative change of mean annual precipitation and the absolute change of mean daily temperature for future peri-

ods. In the figure, each boxplot was constructed using 20 values derived from 20 GCMs. The 51 boxplots in one subgraph represent 51 future periods. The Mann-Kendall trend test revealed that the median of multi-model ensemble precipitation, minimum and maximum temperature all increased significantly (at the significance level of $P = .05$) over time for both emission scenarios. For RCP4.5 (RCP8.5), the ensemble median of annual precipitation increased from 1.4% (1.4%) for 2021–2050 to 6.5% (10.3%) for 2071–2100. RCP8.5 predicted a more rapid increase in precipitation than RCP4.5. In addition, all GCMs predicted increase in daily temperature for both emission scenarios and all future periods. Similar to precipitation, RCP8.5 predicted a larger and more rapid increase in temperature than RCP4.5. For example, RCP4.5 predicted a 1.5 °C increase in minimum temperature for 2021–2050 and a 2.7 °C increase for 2071–2100 in terms of the median of the 20 GCMs, while RCP8.5 predicted a 1.7 °C increase in minimum temperature for 2021–2050 and a 4.8 °C increase for 2071–2100.

Fig. 6 presents the continuous wavelet power spectra of the ensemble medians of future mean annual precipitation, mean daily minimum and maximum temperatures. The results showed that future precipitation and temperature tended to increase with no significant periodicity at the $P = .05$ significance level at the multi-decadal scale, as there is no thick contour within the black outlines. This is expected, as the multiple-year averages of precipitation and temperature were calculated using a moving window approach, the short-term fluctuations such as inter-annual or multi-year variability were filtered. The trend of temporal change in mean annual precipitation and temperature was modeled using the fourth-order polynomial. Table 3 displays the test results of the fitted fourth-order polynomials. From the table, the dr and R^2 values are all above 0.90 and MAE values are very small, which indicate the reasonable performance of the fitted model. F-tests further show that the fitted models were significant at the $P = .05$ significance level.

4.2.2. Changes in seasonal precipitation and temperature

The climate changes in summer and winter mean precipitation and temperature were also analyzed, as the high flow and low flow

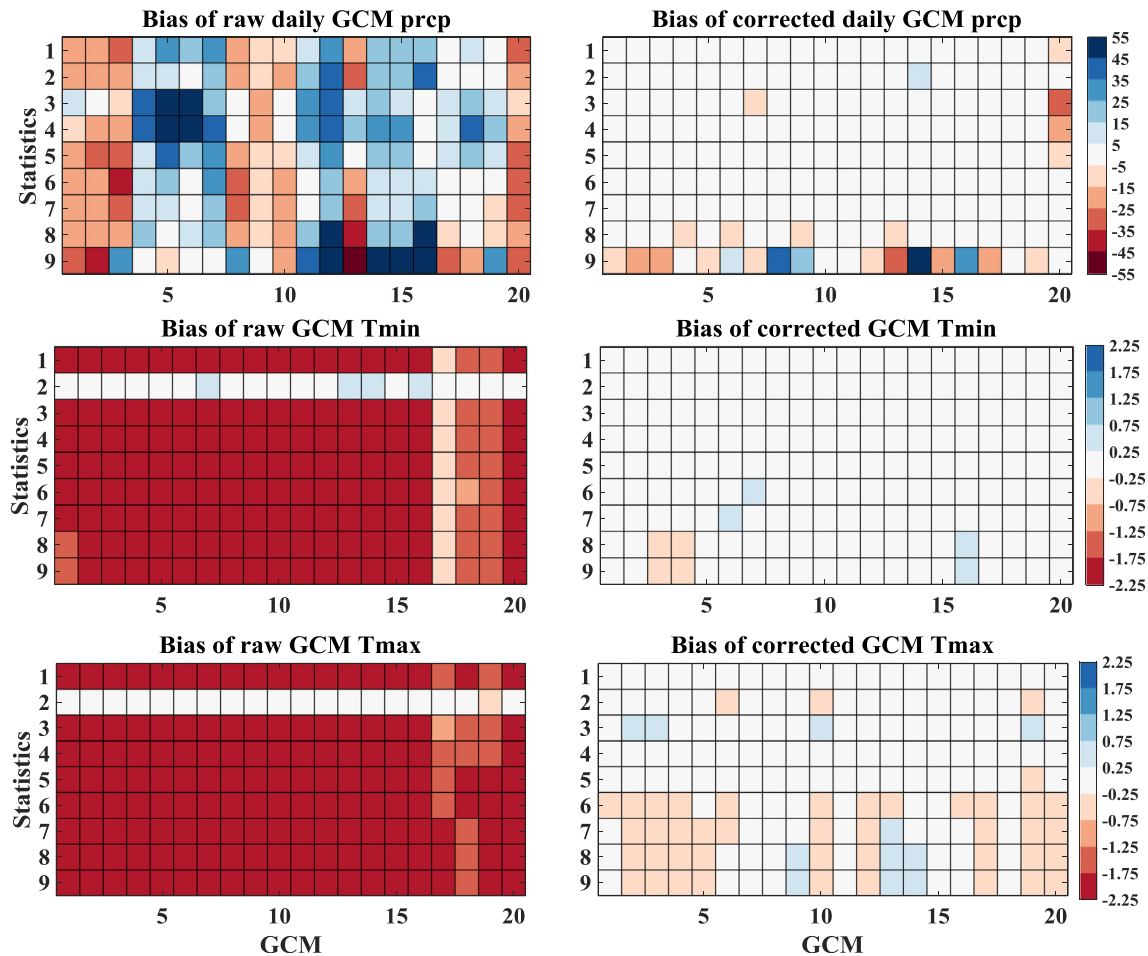


Fig. 4. Biases of raw and corrected GCM outputs in the reference period. The bias is expressed with respect to reproducing nine statistics of observed daily precipitation (prcp), minimum temperature (Tmin) and maximum temperature (Tmax). The statistics include mean, standard deviation, 25th, 50th, 75th, 90th, 95th, and 99th percentiles and maximum value, represented by number 1–9 of y-axis. For precipitation, the bias is represented by the relative difference of statistics between GCM and observation, and is represented by the absolute difference for temperature. X-axis means 20 GCMs.

occur in these two seasons. The figures in this part were presented in the [Supplementary material](#) in order to make the paper in a proper length. [Fig. S1](#) shows that the summer and winter precipitations were all projected to increase for both emission scenarios. For summer, the overall changes of precipitation between the two emission scenarios showed slight difference, with RCP4.5 projecting increases of 1.08% in 2021–2050 and 3.09% in 2071–2100, while RCP8.5 projecting increases of 1.91% in 2021–2050 and 3.42% in 2071–2100. For winter, RCP8.5 predicted more increase than RCP4.5, with the relative change of winter precipitation varying from 8.07% in 2021–2050 to 24.41% in 2071–2100 for RCP4.5, and from 8.69% to 26.20% for RCP8.5. Generally, winter precipitation would likely increase more rapidly than summer precipitation for both emission scenarios. For temperature, only the results of minimum temperature were presented as maximum temperature showed similar changing trends ([Fig. S2](#)). All GCMs projected increases in temperature for both seasons and both emission scenarios. The temperature increased slightly more in summer than in winter for both emission scenarios. Additionally, RCP8.5 projected a larger and more rapid increase in seasonal temperature than RCP4.5, which is coincident with the case of annual mean daily temperature projection. The test and measurement results displayed on the top-left corner of each graph in [Figs. S1 and S2](#) showed that fourth-order polynomial showed reasonable performance in modeling the seasonal climate's temporal variation. Similar to mean annual precipitation and temperature, on the whole,

the ensemble medians of mean seasonal precipitation and temperature did not show significant periodicity at the $P = .05$ significance level tested by wavelet analysis ([Figs. S3 and S4](#)).

4.3. Hydrological impact of climate change

4.3.1. Average hydrographs

[Fig. 7](#) presents the averaged hydrographs simulated using raw and bias corrected GCMs' meteorological data in the reference period (1971–2000), which reflect the performance of bias correction in hydrological modeling. The GCM-simulated streamflows were compared to those simulated using observed meteorological data. The results showed that the streamflows produced using raw GCM data were considerably biased. For example, the simulations using raw GCMs' data reached 9728 m³/s, while the simulation using observed data was just 3278 m³/s for maximum flow. After bias correction, the differences among the GCMs' simulations were remarkably reduced, and the difference between GCM and observed simulations was also considerably reduced. Compared to the large difference (6450 m³/s) for maximum flow before bias correction, the difference was reduced to 1706 m³/s after bias correction (i.e. the simulated maximum flow was 4984 m³/s). Overall, even though biases remain in maximum flows, the bias correction method performed well for most hydrological regimes. Since some biases remained after bias correction, the following section determined the hydrological impacts of climate change in terms of the

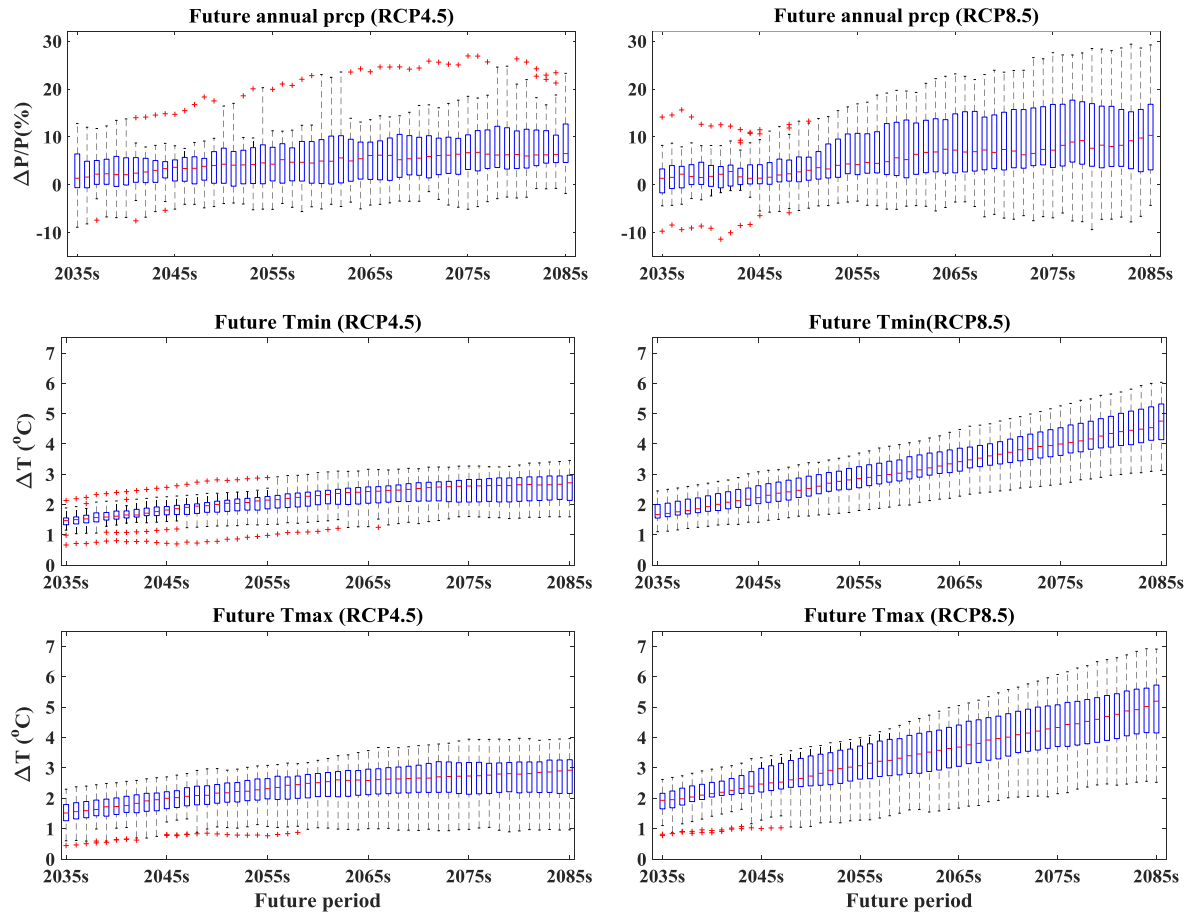


Fig. 5. Future climate change projected by the twenty bias-corrected GCMs for RCP4.5 and RCP8.5. The change in precipitation is expressed by the relative difference of mean annual precipitation between every future period and the reference period, and the change in temperature is expressed by the absolute difference between every future period and the reference period. Note that every boxplot is constructed with the twenty values of the twenty GCMs.

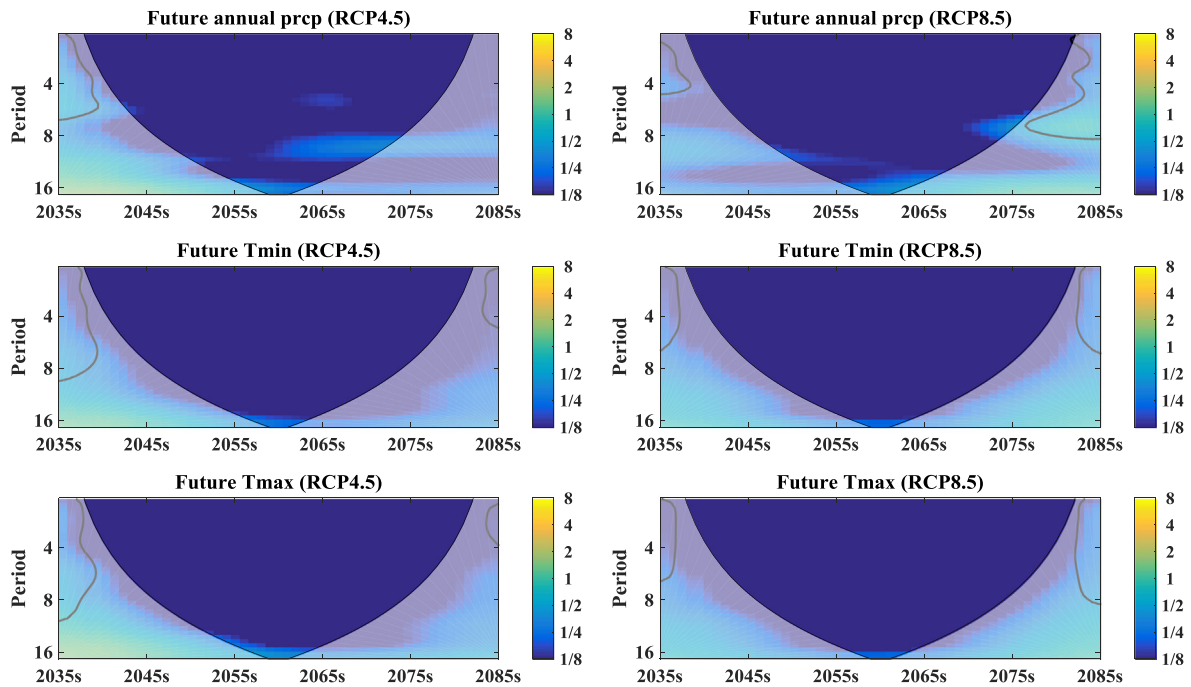


Fig. 6. Continuous wavelet power spectra of the ensemble medians of future mean annual precipitation (prcp), mean daily minimum temperature (Tmin) and mean daily maximum temperature (Tmax). The thick black contours specify the 5% significance level against red noise and cone of influence.

Table 3

Test results on the regression models of the median change of mean annual precipitation (prcp), minimum (Tmin) and maximum (Tmax) temperature using F-test, Willmott's refined index of agreement (*dr*), determination coefficient (R^2), and mean absolute error (MAE). The change is relative change for precipitation while absolute change for temperature.

Scenario	Variable	F-Test		<i>dr</i>	R^2	MAE
		F statistic	p value			
RCP4.5	prcp	327.9	.00	0.91	0.97	0.22
	Tmin	7295.1	.00	0.98	1.00	0.01
	Tmax	3788.9	.00	0.98	1.00	0.02
RCP8.5	prcp	278.9	.00	0.91	0.96	0.43
	Tmin	13067.3	.00	0.99	1.00	0.02
	Tmax	28641.9	.00	0.99	1.00	0.02

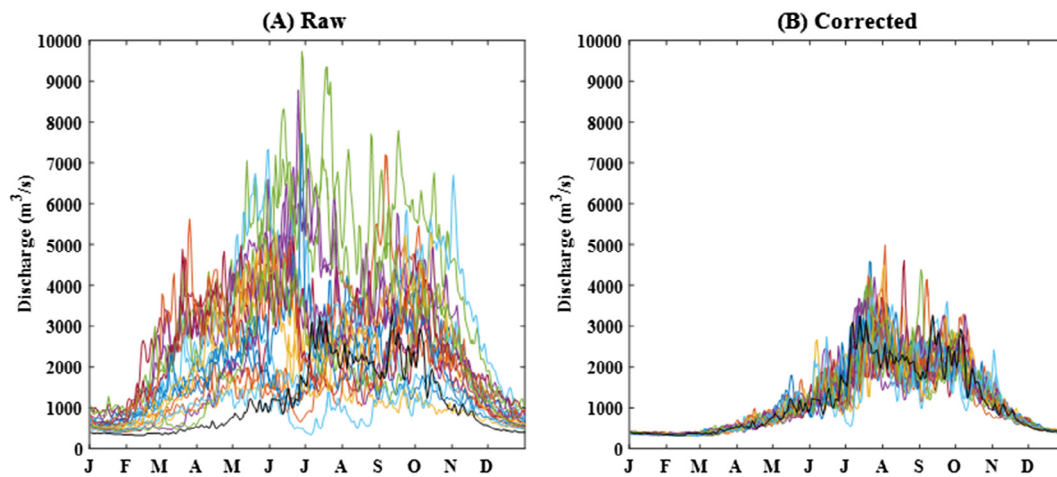


Fig. 7. Hydrographs simulated using (A) raw and (B) corrected GCMs data of the reference period (1971–2000). The thick black line refers to the streamflow simulated using observed meteorological data, the color lines refer to the streamflows simulated using GCM data.

relative change between the model simulated stream flows in future and reference periods. The hydrology in the reference period was simulated using corrected GCM precipitation and temperature.

4.3.2. Change in mean and extreme flows

Fig. 8 presents the relative change of mean, high and low flows for 51 future periods. The Mann-Kendall trend test revealed significant trends (at the $P = .05$ significance level) in all these flows for both emission scenarios. RCP4.5 predicted increasing in mean flows for all future periods in terms of the median of 20 GCMs' projections, while RCP8.5 predicted decreasing in mean flows for the periods between 2036 and 2065, and increasing for other periods. The ensemble medians of mean flow projections changed from 0.6% in 2021–2050 to 5.4% in 2071–2100 for RCP4.5, and from -0.2% to 7.9% for RCP8.5. Overall, the mean flow was predicted to increase more for RCP4.5 before the 2042–2071 period, and then increase more for RCP8.5 in the last half of the 51 future periods (i.e. from 2048 to 2100).

The ensemble medians of high flow was much larger in the first half of 51 future periods for RCP4.5, changing from 5.51% in 2021–2050 to 6.05% in 2046–2075 for RCP4.5, and from 1.67% to 4.06% for RCP8.5. This increase then became larger for RCP8.5 over most of the remaining periods, from 6.20% in 2047–2076 to 7.58% in 2071–2100 for RCP4.5, and from 6.48% to 10.48% for RCP8.5.

Both emission scenarios predicted decreases in low flow for all future periods in terms of the median value of all 20 GCMs. As the time period goes further from 2030 to 2059, RCP4.5 projected less decrease in low flow, while RCP8.5 projected more increase. A significant increasing trend was observed in the relative change of

low flow for RCP4.5, which varied from -7.7% in 2021–2050 to -3.7% in 2071–2100. The relative change for RCP8.5 varied from -7.3% in 2021–2050 to -7.9% in 2071–2100, with a significant decreasing trend. On the whole, RCP8.5 predicted a larger decrease in low flow than RCP4.5.

Similar to precipitation and temperature, the periodicity of ensembles medians of mean flow, high flow and low flow was analyzed using wavelet analysis, and their trend was modeled using fourth-order polynomial. Fig. 9 shows that the mean flow and high flow for both emission scenarios and low flow for RCP4.5 do not exhibit significant periodicity at the $P = .05$ significance level for future periods, while the low flow for RCP8.5 exhibited a 16-year periodicity. But, there are some significant cycles in some years such as a 1–4 year cycle from 2050s to 2060s for mean flow in RCP4.5. In addition, all three metrics (*dr*, MAE and R^2 values) indicated that fourth-order polynomial is a suitable choice in simulating the changing trend of future flow, except for low flow in RCP8.5, whose R^2 value is only 0.22 while others are above 0.85 (Table 4). In addition, fourth-order polynomial performed a bit worse in modeling flow change than modeling climate change. This may be because of the non-linear process from climate to hydrology.

4.4. Uncertainty range of projection

4.4.1. Uncertainty range in climate change projection

Fig. 10 presents the temporal variation of uncertainty in mean annual precipitation, minimum and maximum temperature projections for both emission scenarios in terms of change range of 20 GCMs. On the whole, RCP8.5 showed a large uncertainty in

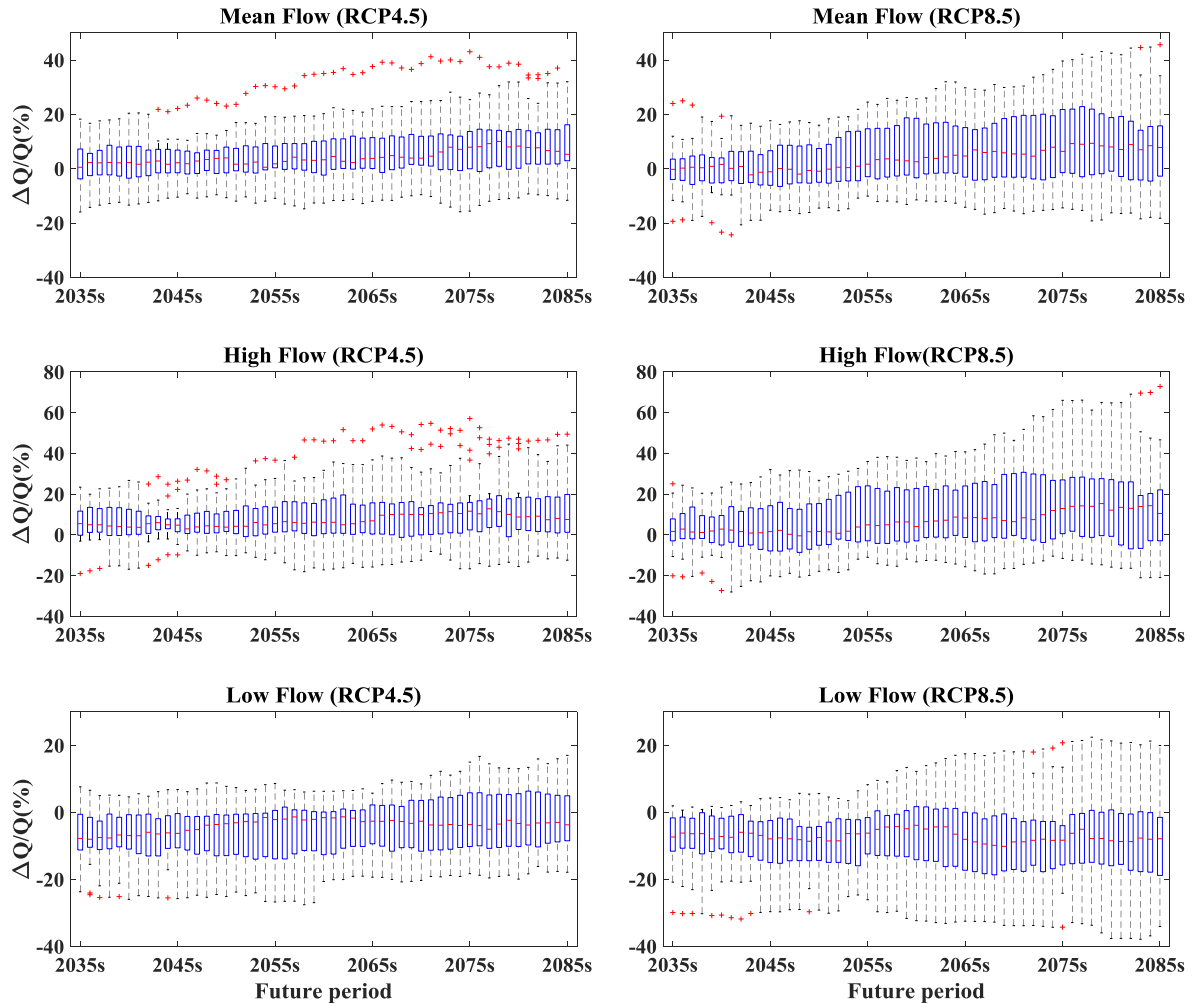


Fig. 8. Relative change of future mean flow, high flow and low flow relative to those in the reference period. Mean flow is defined as the mean value of the 30-year daily discharge time series in each period, high flow it the 95th percentile value and low flow is the 5th percentile value. Note that every boxplot is constructed with the twenty values simulated using the twenty GCM data.

predicting both precipitation and temperature. The uncertainty of precipitation changed from 21.7% in 2021–2050 to 25.1% in 2071–2100 for RCP4.5, and from 12.6% in 2021–2050 to 33.5% in 2071–2100 for RCP8.5. The uncertainty of minimum temperature changed from 0.73 °C in 2021–2050 to 1.86 °C in 2071–2100 for RCP4.5, and from 1.34 °C in 2021–2050 to 2.90 °C in 2071–2100 for RCP8.5. Wavelet analysis showed that the uncertainty variation of precipitation and temperature projections did not contain significant periodicity at the $P = .05$ significance level (Fig. 11). However, a significant increase trend was observed by the Mann-Kendall trend test at the $P = .05$ significance level. Fourth-order polynomials performed reasonably well in terms of simulating the temporal variations of precipitation and temperature uncertainty with the exception of precipitation change under RCP4.5 (Table 5). The d_r and R^2 values for the five reasonable modeling were all above 0.90, and MAE values are very small, while for the worse modeling, the d_r , R^2 values are 0.60, 0.37, respectively. The worse performance of fourth-order polynomials for uncertainty variation of precipitation change under RCP4.5 is due to the ‘abnormal’ projection of MIROC5. MIROC5 projected a much more change in precipitation than other GCMs under RCP4.5 (See Fig. 5), particularly in the periods between 2027 and 2096. A much better performance could be achieved when this climate model was excluded. Probably, a pre-selection of GCMs should be conducted when using multiple GCMs to investigate their uncertainty.

4.4.2. Uncertainty range in streamflow change projection

Similarly, wavelet analysis, Mann-Kendall trend test and regression analysis were also used to analyze the uncertainty of streamflow changes. Fig. 12 displays the temporal variation of uncertainty in mean, high and low flow projections for both emission scenarios. Generally, the high flow showed the largest uncertainty under both emission scenarios, followed by mean and low flows. Specifically, the uncertainty of high flow reached 58.0% in RCP4.5 and 85.4% in RCP8.5, but the uncertainty of mean flow only reached 43.6% in RCP4.5 and 62.7% in RCP8.5, and they were 35.5% in RCP4.5 and 59.0% in RCP8.5 for low flow. Moreover, on the whole, RCP8.5 still projected larger uncertainty than RCP4.5 for all flow statistics. For example, the uncertainty of mean flow was 34.2% for RCP4.5 and 23.6% for RCP8.5 in 2021–2050, and it increased to 43.6% for RCP4.5 and 62.7% for RCP8.5 in 2071–2100. Similar to precipitation and temperature, significant periodicity was not detected by wavelet analysis for all mean, high and low flows at the $P = .05$ significance level (Fig. 13), while a significant increasing trend was observed by the Mann-Kendall trend test at the $P = .05$ significance level. The test results of the fourth-order polynomials fitted in the streamflow changes are shown in Table 6. From the table, the fourth-order polynomials successfully modeled the temporal variation of uncertainty for streamflow change, with most d_r values above 0.70, and R^2 values above 0.76. The fourth-order polynomial model performed a bit worse in simulating the uncertainty

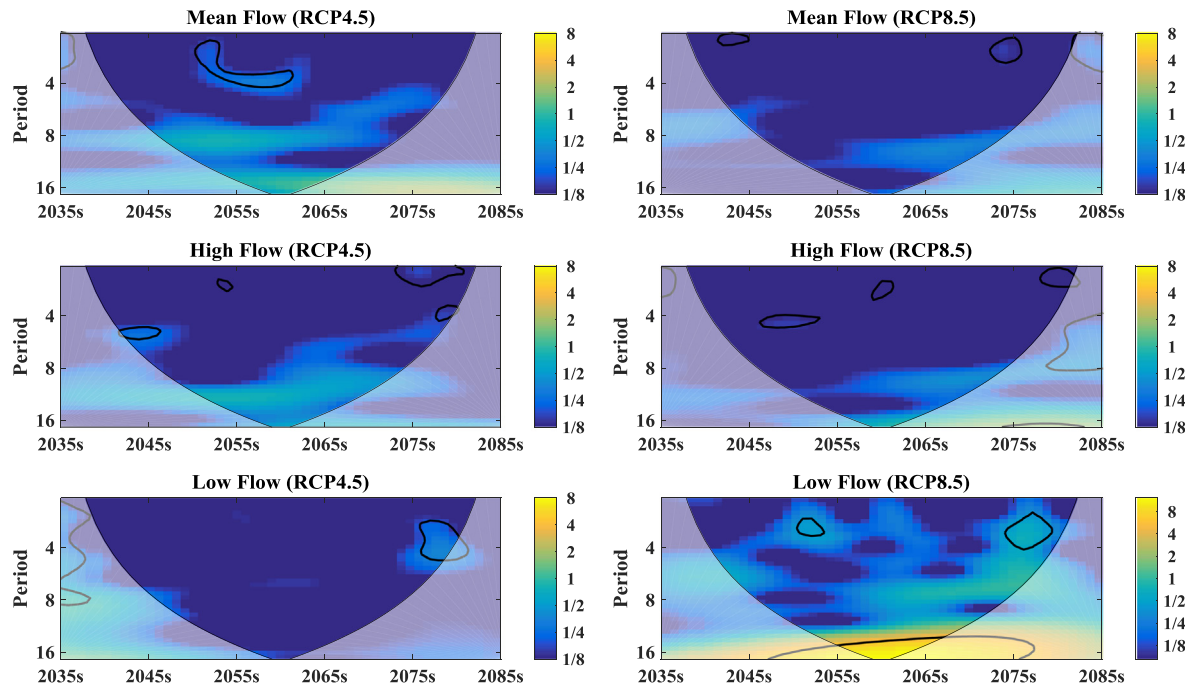


Fig. 9. Continuous wavelet power spectra of the ensemble medians of future mean flow, high flow and low flow. The thick black contours specify the 5% significance level against red noise and cone of influence.

Table 4

Test results on the regression models of the median relative change of mean, high and low flows using F-test, Willmott's refined index of agreement (dr), determination coefficient (R^2), and mean absolute error (MAE).

Scenario	Variable	F-Test		dr	R^2	MAE
		F statistic	p value			
RCP4.5	Mean flow	71.4	.00	0.82	0.86	0.69
	High flow	93.1	.00	0.85	0.89	0.71
	Low flow	138.9	.00	0.87	0.92	0.39
RCP8.5	Mean flow	138.3	.00	0.87	0.92	0.77
	High flow	130.9	.00	0.86	0.92	1.09
	Low flow	3.3	.02	0.60	0.22	1.06

variation in low flow projection under RCP4.5 than the mean and high flows' uncertainty, but it is still statistically significant at $P = .05$ when using F-test.

5. Discussion and conclusion

This study investigated and estimated the temporal variation (mainly long-term) of uncertainty related to the choice of a GCM in hydrological climate change impact studies. The uncertainty was represented by the envelopes of 20 GCMs under two emission scenarios (RCP4.5 and RCP8.5), the temporal variation was presented by 51 future time periods moving from 2021 to 2100 with a 30-year window and 1-year interval, some statistical approaches including wavelet analysis, Mann-Kendall trend test and polynomial regression analysis were used to analyze the temporal variation.

The precipitation and temperature were projected to increase significantly in the future, but with great uncertainty. For example, the ensemble median of precipitation predictions increased from 1.4% in 2021–2050 to 6.5% in 2071–2100 for RCP4.5, and from 1.4% to 10.3% for RCP8.5, but the projection uncertainty reached 21.7% in 2021–2050 and 25.1% in 2071–2100 for RCP4.5, and reached 12.6% in 2021–2050 and 33.5% in 2071–2100 for RCP8.5. In addition, the projection uncertainty under a high greenhouse

gas emission scenario (RCP8.5) was found to be larger than that under a low greenhouse gas emission scenario (RCP4.5). This means these GCMs behaved more differently from each other under higher emission scenario in the future despite they were constructed under same radiative forcing.

Wavelet analysis showed insignificant periodicity for the ensemble medians of climatic and hydrological variables and their uncertainty at the $P = .05$ significance level, with the exception of low flow in RCP8.5, which showed a 16-year periodicity. This is because the 30-year moving average used in this study filtered the inter-annual or multi-year variability/fluctuation. In order to examine if there was any short-term periodicity, wavelet analysis was further applied to analyze the yearly variation of climatic and hydrological variables in 2021–2100. The results showed that the yearly time series of future annual precipitation had a 4-year cycle in RCP4.5, and 8-year, 19-year cycles in RCP8.5, and future temperature had no significant periodicity at the $P = .05$ significance level. The yearly variation of future mean flow had a 5-year cycle in RCP4.5, and 20-year cycle in RCP8.5. However, these small periodicities were filtered out by the 30-year moving window, so in the long-term, no significant periodicity was observed.

The fourth-order polynomial is a reasonable choice for modeling the temporal variation of climatic and hydrological changes as well as their uncertainty. The climate system is highly nonlinear,

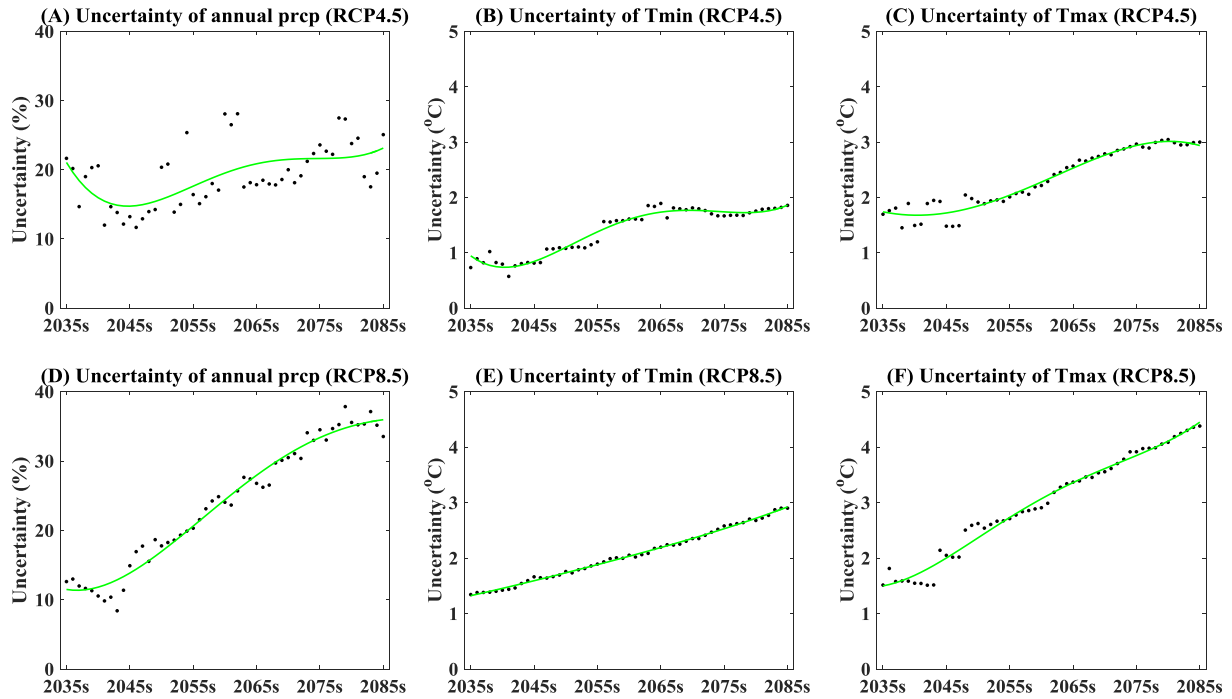


Fig. 10. Quantification of the temporal variation of uncertainty (i.e. prediction range) in precipitation and temperature predictions for RCP4.5 and RCP8.5. Scattered point means the uncertainty value in each future period, and green line means the fourth-order polynomial model fitted to the scatter points in each graph.

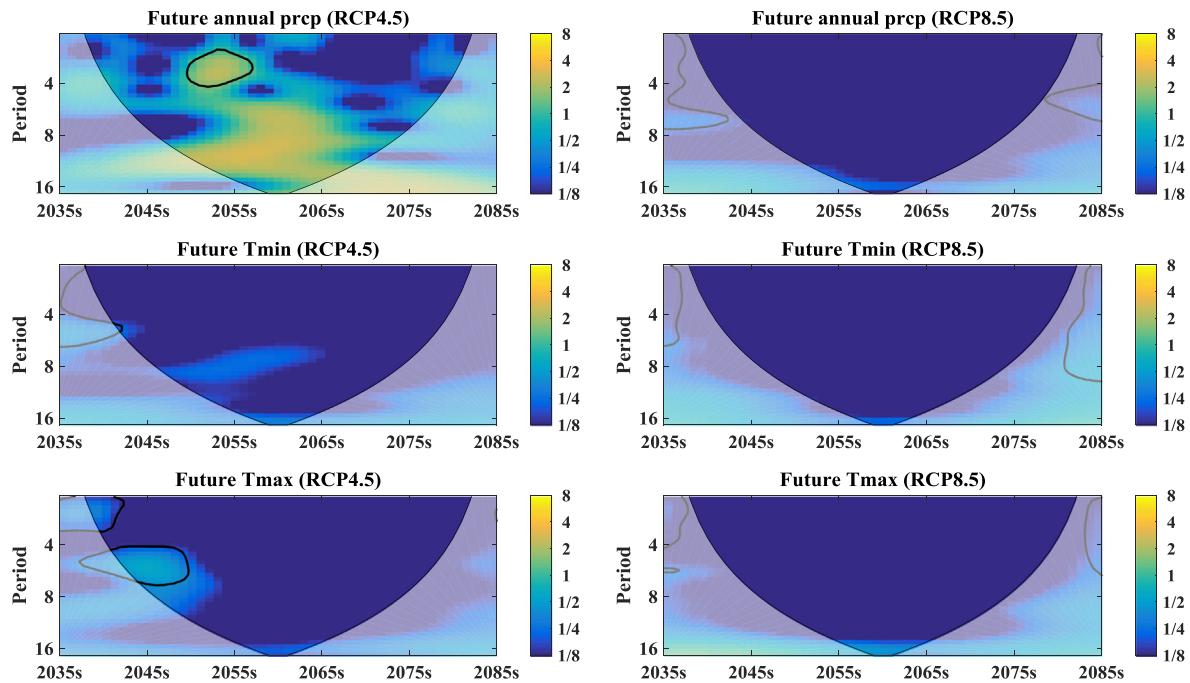


Fig. 11. Continuous wavelet power spectra of the uncertainty (i.e. prediction range) in precipitation and temperature prediction for RCP4.5 and RCP8.5. The thick black contours specify the 5% significance level against red noise and cone of influence.

and change is often abrupt and episodic rather than slow and gradual (Rial et al., 2004; Bond et al., 2013); modeling the abrupt changes can be really challenging and also makes little sense, so this study chose to use a 30-year moving window to filter out the small fluctuations and changes and highlight the long-term changing trend. Besides, changes in climate system tend to be non-stationary due to the increasing anthropogenic activity, from this perspective, a nonlinear model instead of a linear model is more

reasonable to model the temporal variations of climatic and hydrological ensemble medians, and their uncertainty. The fourth-order polynomial was chosen in this case study based on previous studies (e.g. Hawkins and Sutton, 2009, 2011). The fourth-order polynomial performed reasonably well in simulating the temporal variation of ensemble medians of climate and hydrology as well as their uncertainty, with the exception of modeling low flow magnitude in RCP8.5, precipitation uncertainty in RCP4.5 and low flow

Table 5
Test results on the regression models of the uncertainty in mean annual precipitation (prcp), minimum (Tmin) and maximum (Tmax) temperature projections using F-test, Willmott’s refined index of agreement (*dr*), determination coefficient (*R*²), and mean absolute error (MAE).

Scenario	Variable	F-Test		<i>dr</i>	<i>R</i> ²	MAE
		F statistic	p value			
RCP4.5	prcp	6.8	.00	0.60	0.37	2.90
	Tmin	215.0	.00	0.91	0.95	0.07
	Tmax	216.0	.00	0.91	0.95	0.08
RCP8.5	prcp	400.5	.00	0.93	0.97	1.10
	Tmin	3185.7	.00	0.97	1.00	0.02
	Tmax	585.5	.00	0.95	0.98	0.08

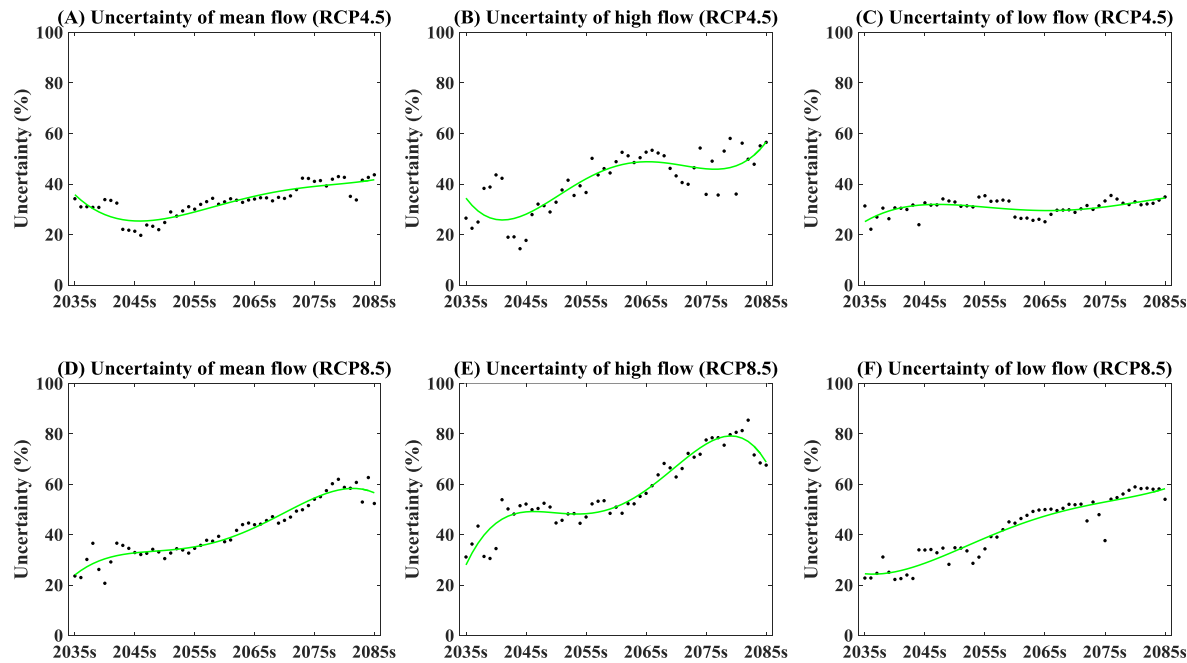


Fig. 12. Quantification of the temporal variation of uncertainty (i.e. prediction range) in mean flow, high flow and low flow predictions for RCP4.5 and RCP8.5. Scattered point means the uncertainty value in each future period, and green line means the fourth-order polynomial model fitted to the scatter points in each graph.

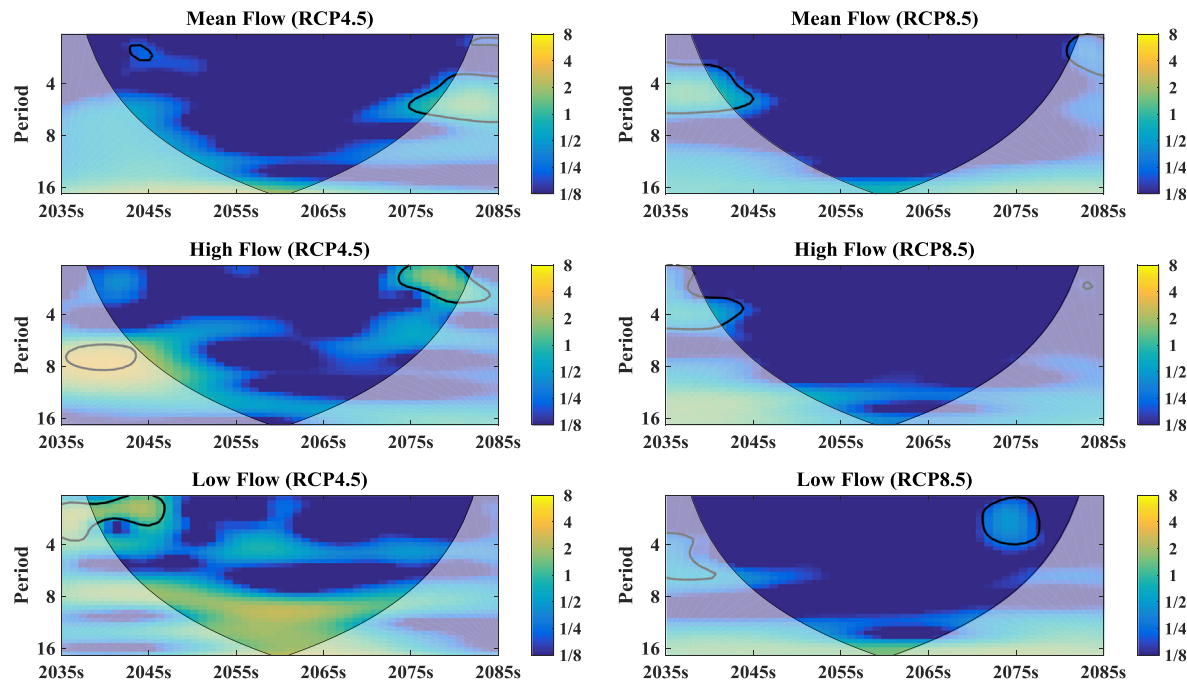


Fig. 13. Continuous wavelet power spectra of the uncertainty (i.e. prediction range) in mean flow, high flow and low flow predictions for RCP4.5 and RCP8.5. The thick black contours specify the 5% significance level against red noise and cone of influence.

Table 6

Test results on the regression models of the uncertainty in mean, low and high flows projections using F-test, Willmott's refined index of agreement (*dr*), determination coefficient (R^2), and mean absolute error (MAE).

Scenario	Variable	F-Test		<i>dr</i>	R^2	MAE
		F statistic	p value			
RCP4.5	Mean flow	38.2	.00	0.74	0.77	2.45
	High flow	19.0	.00	0.71	0.62	5.33
	Low flow	5.2	.00	0.62	0.31	1.86
RCP8.5	Mean flow	149.0	.00	0.88	0.93	2.15
	High flow	134.2	.00	0.87	0.92	3.00
	Low flow	97.2	.00	0.86	0.89	2.88

uncertainty in RCP4.5. The worse performance in modeling precipitation uncertainty in RCP4.5 was because one GCM (MIROC5) projected much more precipitation than all other GCMs. The worse performance in modeling low flow magnitude in RCP8.5 and low flow uncertainty in RCP4.5 may be because of the difficulty in accurately simulating low flow by the hydrological model in this basin.

It is worth mentioning that there are some limitations to the approach presented in this study. One is that only one downscaling method was adapted for downscaling purpose. Downscaling method is usually considered to be another contributor to uncertainty in climate change impact studies (Wilby and Harris, 2006; Chen et al., 2011b). Among the large community of downscaling methods, varying from dynamical to statistical, it is less confident to say which method is preferable than others (Teng et al., 2012), every method has its advantages as well as disadvantages. This study chose a hybrid downscaling method that combines LOCI and DT to take account of correction in both wet-day frequency and wet-day precipitation distribution.

In addition, only one hydrological model was used in this study, even though hydrological model is also an important source of uncertainty in hydrological climate change impact studies (Jiang et al., 2007; Dibike and Coulibaly, 2007). This thoughtlessness is also because the aim of the study is mainly to investigate the uncertainty related to the choice of a GCM. On the other hand, compared to GCM and downscaling method, the choice of hydrological models can have less influence on the hydrological projection (Wilby and Harris, 2006; Chen et al., 2011b).

In this study, the HMETs model calibrated using NSE as criterion was used for simulating discharge in the future, after compared with two other hydrological models (GR4J model (Perrin et al., 2003) and Xinanjiang model (XAJ) (Zhao, 1992; Zeng et al., 2016)) calibrated using NSE and Kling-Gupta efficiency (KGE, defined by Gupta et al., 2009) as criteria. On the whole, the HMETs model calibrated using NSE performed best in terms of reproducing the observed streamflow, while the GR4J and XAJ models can yield approximately same efficiency values as HMETs model if NSE or KGE was selected as criterion, but they reproduced low flow with greater error. The HMETs model calibrated using KGE as criterion also failed to capture the variation of low flow.

Moreover, the uncertainty of climate change impacts may vary among watersheds due to different hydro-climatologic characteristics and combinations between climate simulations and regional conditions (Kay et al., 2009; Jung et al., 2012). It would be worthwhile to apply the methodology presented here to other watersheds to extract more generalized conclusions.

Acknowledgements

This work was partially supported by the National Natural Science Foundation of China (Grant No. 51779176, 51525902, 51539009) and the Thousand Youth Talents Plan from the Organization Department of CCP Central Committee (Wuhan University, China). The authors would like to acknowledge the contribution of the World Climate Research Program Working Group on Cou-

pled Modelling, and to thank climate modeling groups for making available their respective climate model outputs. The authors wish to thank the China Meteorological Data Sharing Service System and the Bureau of Hydrology of the Changjiang Water Resources Commission for providing dataset for the Hanjiang River watershed.

Appendix A. Supplementary data

Supplementary data associated with this article can be found, in the online version, at <https://doi.org/10.1016/j.jhydrol.2017.11.004>.

References

- Ahmadalipour, A., Moradkhani, H., Rana, A., 2017. Accounting for downscaling and model uncertainty in fine-resolution seasonal climate projections over the Columbia river basin. *Clim. Dyn.*, 1–17.
- Arsenault, R., Poulin, A., Cote, P., Brissette, F., 2014. Comparison of stochastic optimization algorithms in hydrological model calibration. *J. Hydrol. Eng.* 19 (7), 1374–1384.
- Bae, D.H., Jung, I.W., Lettenmaier, D.P., 2011. Hydrologic uncertainties in climate change from IPCC AR4 GCM simulations of the Chungju Basin, Korea. *J. Hydrol.* 401 (1–2), 90–105.
- Bates, D.M., Watts, D.G., 1988. *Nonlinear Regression Analysis and Its Applications*. Wiley.
- Bond, T.C., Doherty, S.J., Fahey, D.W., Forster, P.M., Bernsten, T., Deangelo, B.J., et al., 2013. Bounding the role of black carbon in the climate system: a scientific assessment. *J. Geophys. Res.-Atmos.* 118 (11), 5380–5552.
- Brigode, P., Brissette, F., Caya, D., Nicault, A., Perreault, L., Kuentz, A., et al., 2015. Flood variability over 1871–2012 in Northern Québec: comparison of hydrological reconstructions based on tree-rings and on geopotential height field reanalysis. *European Geosciences Union (Vol.17)*.
- Brigode, P., Oudin, L., Perrin, C., 2013. Hydrological model parameter instability: a source of additional uncertainty in estimating the hydrological impacts of climate change? *J. Hydrol.* 476, 410–425.
- Brisson, E., Demuzere, M., Willems, P., van Lipzig, N., 2015. Assessment of natural climate variability using a weather generator. *Clim. Dynam.* 44 (1–2), 495–508.
- Chen, H., Xu, C.-Y., Guo, S.L., 2012. Comparison and evaluation of multiple GCMs, statistical downscaling and hydrological models in the study of climate change impacts on runoff. *J. Hydrol.* 434–435, 36–45.
- Chen, J., St-Denis, B.G., Brissette, F.P., Lucas-Picher, P., 2016. Using natural variability as a baseline to evaluate the performance of bias correction methods in hydrological climate change impact studies. *J. Hydrometeorol.* 17 (8), 2155–2174.
- Chen, J., Brissette, F.P., Chaumont, D., Braun, M., 2013. Performance and uncertainty evaluation of empirical downscaling methods in quantifying the climate change impacts on hydrology over two North American river basins. *J. Hydrol.* 479, 200–214.
- Chen, J., Brissette, F.P., Leconte, R., 2011a. Uncertainty of downscaling method in quantifying the impact of climate change on hydrology. *J. Hydrol.* 401 (3–4), 190–202.
- Chen, J., Brissette, F.P., Poulin, A., Leconte, R., 2011b. Overall uncertainty study of the hydrological impacts of climate change for a Canadian watershed. *Water Resour. Res.* 47, W12509. <https://doi.org/10.1029/2011wr010602>.
- De Moortel, I., Munday, S.A., Hood, A.W., 2004. Wavelet analysis: the effect of varying basic wavelet parameters. *Solar Phys.* 222, 203–228.
- Dibike, Y.B., Coulibaly, P., 2007. Validation of hydrological models for climate scenario simulation: the case of Saguenay watershed in Quebec. *Hydrol. Process.* 21 (23), 3123–3135.
- Emetadi, H., Samadi, S., Sharifikia, M., 2014. Uncertainty analysis of statistical downscaling models using general circulation model over an international wetland. *Clim. Dynam.* 42 (11–12), 2899–2920.
- Fang, G.H., Yang, J., Chen, Y.N., Zhang, S.H., Deng, H.J., Liu, H.M., De Maeyer, P., 2015. Climate change impact on the hydrology of a typical watershed in the Tianshan Mountains. *Adv. Meteorol.* <https://doi.org/10.1155/2015/960471>.

- Eregno, F.E., Xu, C.-Y., Kitterød, N.-O., 2013. Modeling hydrological impacts of climate change in different climatic zones. *Int. J. Clim. Change Strategies Manage.* 5 (3).
- Ferraro, M.B., Colubi, A., Gonzalez-Rodriguez, G., Coppi, R., 2011. A determination coefficient for a linear regression model with imprecise response. *Environmetrics* 22 (4), 516–529.
- Ficklin, D.L., Letsinger, S.L., Stewart, I.T., Maurer, E.P., 2016. Assessing differences in snowmelt-dependent hydrologic projections using CMIP3 and CMIP5 climate forcing data for the western United States. *Hydrol. Res.* 47 (2), 483–500.
- Fowler, H.J., Blenkinsop, S., Tebaldi, C., 2007. Linking climate change modelling to impacts studies: recent advances in downscaling techniques for hydrological modelling. *Int. J. Climatol.* 27 (12), 1547–1578.
- Grinsted, A., Moore, J., Jevrejeva, S., 2004. Application of the cross wavelet transform and wavelet coherence to geophysical time series. *Nonlinear Processes Geophys.* 11 (5–6), 561–566.
- Gupta, H.V., Kling, H., Yilmaz, K.K., Martinez, G.F., 2009. Decomposition of the mean squared error and NSE performance criteria: implications for improving hydrological modelling. *J. Hydrol.* 377 (1–2), 80–91.
- Hansen, N., Ostermeier, A., 2001. Completely derandomized self-adaptation in evolution strategies. *Evol. Comput.* 9 (2), 159–195.
- Hawkins, E., Sutton, R., 2009. The potential to narrow uncertainty in regional climate predictions. *Bull. Am. Meteorol. Soc.* 90 (8), 1095–1107.
- Hawkins, E., Sutton, R., 2011. The potential to narrow uncertainty in projections of regional precipitation change. *Clim. Dynam.* 37 (1–2), 407–418.
- IPCC, 2013. *Climate Change 2013: The Physical Science Basis. Contribution of Working Group I to the Fifth Assessment Report of the Intergovernmental Panel on Climate Change* [Stocker, T.F., Qin, G.-K., Plattner, M., Tignor, S.K., Allen, J., Boschung, A., Nauels, Y., Xia, V. Bex and P.M. Midgley (eds.)]. Cambridge University Press, Cambridge, United Kingdom and New York, NY, USA, 1535 pp.
- Jenkins, G., Lowe, J., 2003. Handling uncertainties in the UKCIP02 scenarios of climate change. Hadley Cent.tech.note No.
- Jiang, T., Chen, Y.D., Xu, C.-Y., Chen, X.H., Chen, X., Singh, V.P., 2007. Comparison of hydrological impacts of climate change simulated by six hydrological models in the Dongjiang Basin, South China. *J. Hydrol.* 336 (3–4), 316–333.
- Jung, I.W., Moradkhani, H., Chang, H., 2012. Uncertainty assessment of climate change impacts for hydrologically distinct river basins. *J. Hydrol.* 466, 73–87.
- Kay, A.L., Davies, H.N., Bell, V.A., Jones, R.G., 2009. Comparison of uncertainty sources for climate change impacts: flood frequency in England. *Clim. Change* 92 (1–2), 41–63.
- Kendall, M.G., 1975. *Rank Correlation Methods*. Charles Griffin, London.
- Khan, M.S., Coulibaly, P., Dibike, Y., 2006. Uncertainty analysis of statistical downscaling methods using Canadian Global Climate Model predictors. *Hydrol. Process.* 20 (14), 3085–3104.
- Kharin, V.V., Zwiers, F.W., Zhang, X., Hegerl, G.C., 2013. Changes in temperature and precipitation extremes in the ipcc ensemble of global coupled model simulations. *Clim. Change* 119 (2), 345–357.
- Li, L., Diallo, I., Xu, C.-Y., Stordal, F., e. Hydrological projections under climate change in the near future by RegCM4 in Southern Africa using a large-scale hydrological model. *J. Hydrol.* 528, 1–16.
- Mann, H.B., 1945. Non-Parametric Tests against Trend. *Econometrica* 13, 245–259.
- Maraun, D., 2013. Bias correction, quantile mapping, and downscaling: revisiting the inflation issue. *J. Clim.* 26, 2137–2143.
- Martel, J.-L., Demeester, K., Brissette, F., Poulin, A., Arsenault, R., 2017. HMETS - A simple and efficient hydrology model for teaching hydrological modelling, flow forecasting and climate change impacts. *Int. J. Eng. Educ.* 33 (4), 1307–1316.
- Maurer, E.P., 2007. Uncertainty in hydrologic impacts of climate change in the Sierra Nevada, California, under two emissions scenarios. *Clim. Change* 82 (3–4), 309–325.
- Mpelasoka, F.S., Chiew, F.H.S., 2009. Influence of rainfall scenario construction methods on runoff projections. *J. Hydrometeorol.* 10 (5), 1168–1183.
- Minville, M., Brissette, F., Leconte, R., 2008. Uncertainty of the impact of climate change on the hydrology of a nordic watershed. *J. Hydrol.* 358 (1–2), 70–83.
- Nobrega, M.T., Collischonn, W., Tucci, C.E.M., Paz, A.R., 2011. Uncertainty in climate change impacts on water resources in the Rio Grande Basin, Brazil. *Hydrol. Earth Syst. Sci.* 15 (2), 585–595.
- Perrin, C., Michel, C., Andreassian, V., 2003. Improvement of a parsimonious model for streamflow simulation. *J. Hydrol.* 279 (1–4), 275–289.
- Poulin, A., Brissette, F., Leconte, R., Arsenault, R., Malo, J.S., 2011. Uncertainty of hydrological modelling in climate change impact studies in a Canadian, snow-dominated river basin. *J. Hydrol.* 409 (3–4), 626–636.
- Prudhomme, C., Davies, H., 2009. Assessing uncertainties in climate change impact analyses on the river flow regimes in the UK. Part 2: future climate. *Clim. Change* 93 (1–2), 197–222.
- Ramsey, J.B., 1999. Regression over timescale decompositions: a sampling analysis of distributional properties. *Econ. Syst. Res.* 11 (2), 163–183.
- Rial Sr., J.A., Pielker, R.A., Beniston, M., Claussen, M., Canadell, J., Cox, P., et al., 2004. Nonlinearities, feedbacks and critical thresholds within the Earth's climate system. *Clim. Change* 65 (1–2), 11–38.
- Rowell, D.P., 2006. A demonstration of the uncertainty in projections of UK climate change resulting from regional model formulation. *Clim. Change* 79 (3–4), 243–257.
- Samadi, S., Wilson, C.A.M.E., Moradkhani, H., 2013. Uncertainty analysis of statistical downscaling models using Hadley Centre Coupled Model. *Theor. Appl. Climatol.* 114 (3–4), 673–690.
- Schmidli, J., Frei, C., Vidale, P.L., 2006. Downscaling from GCM precipitation: a benchmark for dynamical and statistical downscaling methods. *Int. J. Climatol.* 26 (5), 679–689.
- Sillmann, J., Kharin, V.V., Zhang, X.B., 2013. Climate extremes indices in the cmip5 multi-model ensemble: part 1. *J. Geophys. Res. Atmos.* 118, 1–18.
- Teng, J., Vaze, J., Chiew, F.H.S., Wang, B., Perraud, J.M., 2012. Estimating the relative uncertainties sourced from GCMs and hydrological models in modeling climate change impact on runoff. *J. Hydrometeorology* 13 (1), 122–139.
- Torrence, C., Compo, G.P., 1998. A practical guide to wavelet analysis. *Bull. Am. Meteorol. Soc.* 79 (1), 61–78.
- Troin, M., Arsenault, R., Brissette, F., 2015. Performance and uncertainty evaluation of snow models on snowmelt flow simulations over a Nordic Catchment (Mistassibi, Canada). *Hydrology* 2 (4), 289–317.
- Wang, Y.K., Wang, D., Wu, J.C., 2015. Assessing the impact of Danjiangkou reservoir on ecohydrological conditions in Hanjiang River, China. *Ecol. Eng.* 81, 41–52.
- Wilby, R.L., Harris, I., 2006. A framework for assessing uncertainties in climate change impacts: low-flow scenarios for the River Thames, UK. *Water Resour. Res.* 42 (2). <https://doi.org/10.1029/2005WR004065>.
- Wilby, R.L., Hassan, H., Hanaki, K., 1998. Statistical downscaling of hydrometeorological variables using general circulation model output. *J. Hydrol.* 205 (1–2), 1–19.
- Willmott, C.J., Matsuura, K., 2005. Advantages of the mean absolute error (MAE) over the root mean square error (RMSE) in assessing average model performance. *Clim. Res.* 30 (1), 79–82.
- Willmott, C.J., Robeson, S.M., Matsuura, K., 2012. A refined index of model performance. *Int. J. Climatol.* 32 (13), 2088–2094.
- Willmott, C.J., Robeson, S.M., Matsuura, K., Ficklin, D.L., 2015. Assessment of three dimensionless measures of model performance. *Environ. Modell. Software* 73, 167–174.
- Xu, C.Y., 1999. From GCMs to river flow: a review of downscaling methods and hydrologic modelling approaches. *Prog. Phys. Geogr.* 23 (2), 229–249.
- Xu, J., Chen, Y., Lu, F., Li, W., Zhang, L., Hong, Y., 2011. The Nonlinear trend of runoff and its response to climate change in the Aksu River, western China. *Int. J. Climatol.* 31 (5), 687–695.
- Xu, Y.P., Yu, C.F., Zhang, X.J., Zhang, Q.Q., Xu, X., 2012. Design rainfall depth estimation through two regional frequency analysis methods in Hanjiang River Basin, China. *Theor. Appl. Climatol.* 107 (3–4), 563–578.
- Zeng, Q., Chen, H., Xu, C.-Y., Jie, M.X., Hou, Y.K., 2016. Feasibility and uncertainty of using conceptual rainfall runoff models in design flood estimation. *Hydrol. Res.* 47 (4), 701–717.
- Zhang, H., Huang, G.H., Wang, D.L., Zhang, X.D., 2011. Uncertainty assessment of climate change impacts on the hydrology of small prairie wetlands. *J. Hydrol.* 396 (1–2), 94–103.
- Zhao, R.J., 1992. The Xinanjiang Model Applied in China. *J. Hydrol.* 135 (1–4), 371–381.